

Effectively modulating spatial vortex four-wave mixing in a diamond atomic system

Nuo Ba(巴诺), Ming-Qi Jiang(姜明奇), Jin-You Fei(费金友), Dan Wang(王丹), Hai-Lin Jiang(蒋海林), Lei Wang(王磊), and Hai-Hua Wang(王海华)

Citation: Chin. Phys. B, 2024, 33 (**4**): 044202. DOI: 10.1088/1674-1056/ad0771
Journal homepage: http://cpb.iphy.ac.cn; http://iopscience.iop.org/cpb

What follows is a list of articles you may be interested in

Absorption spectra and enhanced Kerr nonlinearity in a four-level system

Hao-Jie Huangfu(皇甫浩杰), Ying-Jie Du(杜英杰), and Ai-Hua Gao(高爱华)
Chin. Phys. B, 2023, 32 (**11**): 114214. DOI: 10.1088/1674-1056/ad0622

Generation of spectrally uncorrelated biphotons via fiber nonlinear quantum interference

Zhengtong Wei(卫正统), Chuan Qu(瞿川), Tian'an Wu(吴天安), Yuanyuan Li(李媛媛), Bo Li(李博), and Shenghai Zhang(张胜海)
Chin. Phys. B, 2023, 32 (**6**): 064202. DOI: 10.1088/1674-1056/acb767

Dynamic manipulation of probe pulse and coherent generation of beating signals based on tunneling-induced inference in triangular quantum dot molecules

Nuo Ba(巴诺), Jin-You Fei(费金友), Dong-Fei Li(李东飞), Xin Zhong(钟鑫), Dan Wang(王丹), Lei Wang(王磊), Hai-Hua Wang(王海华), Qian-Qian Bao(鲍倩倩)
Chin. Phys. B, 2020, 29 (**3**): 034204. DOI: 10.1088/1674-1056/ab683d

Observation of multi-Raman gain resonances in rubidium vapor

Jun Liu(刘俊), Dong Wei(卫栋), Jin-wen Wang(王金文), Ya Yu(余娅), Hua-jie Hu(胡华杰), Hong Gao(高宏), Fu-li Li(李福利)
Chin. Phys. B, 2016, 25 (**11**): 114204. DOI: 10.1088/1674-1056/25/11/114204

Strong violations of locality by testing Bell's inequality with improved entangled-photon systems

Wang Yao (王尧), Fan Dai-He (樊代和), Guo Wei-Jie (郭伟杰), Wei Lian-Fu (韦联福)
Chin. Phys. B, 2015, 24 (**8**): 084203. DOI: 10.1088/1674-1056/24/8/084203

Effectively modulating spatial vortex four-wave mixing in a diamond atomic system

Nuo Ba(巴诺)[1,†], Ming-Qi Jiang(姜明奇)[1], Jin-You Fei(费金友)[1], Dan Wang(王丹)[1], Hai-Lin Jiang(蒋海林)[2], Lei Wang(王磊)[2,‡], and Hai-Hua Wang(王海华)[2]

[1] *National Demonstration Center for Experimental Physics Education, College of Physics, Jilin Normal University, Siping* 136000, *China*
[2] *College of Physics, Jilin University, Changchun* 130012, *China*

(Received 19 June 2023; revised manuscript received 23 October 2023; accepted manuscript online 27 October 2023)

Due to the spatial characteristics of orbital angular momentum, vortex fields can be applied in the fields of quantum storage and quantum information. We study the realization of spatially modulated vortex fields based on four-wave mixing in a four-level atomic system with a diamond structure. The intensity and spiral phase of the vortex field are effectively transferred to the generated four-wave mixing field. By changing the detuning of the probe field, the phase and intensity of the generated vertex four-wave mixing field can be changed. When the probe field takes a large detuning value, the spatial distribution of the intensity and phase of the vertex four-wave mixing field can be effectively tuned by adjusting the Rabi frequency or detuning value of the coupled field. At the same time, we also provide a detailed explanation based on the dispersion relationship, and the results agree well with our simulation results.

Keywords: coherent optical effects, four-wave mixing, orbital angular momentum

PACS: 42.50.Gy, 42.50.Wk, 37.10.Vz **DOI:** 10.1088/1674-1056/ad0771

1. Introduction

Atomic coherence refers to the interference phenomenon that when light interacts with matter, different energy levels of atoms become mutually correlated, and then quantum interference occurs in different transition paths. Atomic coherence can effectively tune the nonlinear optical properties of atomic systems or solid media, leading to the emergence of important quantum interference phenomena such as coherent population trapping (CPT),[1] lasing without inversion (LWI)[2,3] and electromagnetically induced transparency (EIT).[4,5] EIT is a typical atomic coherence phenomenon that uses a strong coherent field to couple the two energy levels of an atom, so that the absorption of the probe field is reduced or even transparent at the two-photon resonance. Because EIT technology can make the signal light pass through the medium without absorption and accompanied by a large nonlinear refractive index, the realization of high-efficiency four-wave mixing (FWM) by EIT has been widely studied.[6–10] Deng *et al*. proposed theoretically how to obtain optically coherent FWM by using a pump field with slow light group velocity.[11] Wu *et al*. gave the high-efficiency FWM field by using EIT-induced suppression of nonlinear absorptions.[12] Wu *et al*. obtained the FWM field with the same group velocity and pulse shape as those of the input pump field based on multiphoton destructive interference.[13] Xiao *et al*. studied the coexisting FWM and six-wave mixing channels via dual-EIT windows in a Y-type atomic system.[14]

Vortex light is a kind of light field with special phase structure and peculiar topological characteristics, whose wavefront phase contains the spiral phase factor related to the orbital angular momentum (OAM) and the light intensity is zero at the center.[15,16] In recent years, because the optical vortex field has practical application in the manipulation of OAM for information processing, there has been much research work on vortex optics.[17–19] In 2012, Walker and colleagues used FWM technology to transfer the orbital angular momentum of pump light to the generated FWM light in Rb vapor.[20] In 2014, Ding *et al*. made two back-propagating pump and signal lights carrying orbital angular momentum interact with an M-type ^{85}Rb atomic ensemble. As a result, a gear-shaped interference pattern was observed in the generated FWM light, and the input signal light was doughnut shaped.[21] In 2018, Wang *et al*. studied the interference image of vortex light based on the photonic band gap structure and found that the interference image of vortex detection can be distorted by changing the input angle of the vortex field.[22] In 2019, Jing *et al*. obtained multiplexed continuous variable entanglements of orbital angular momentum by using FWM in hot atomic vapor.[23] In recent years, people have used a vortex field to obtain an adjustable spatially correlated FWM field in various atomic models,[24–26] semiconductor nanostructures[27–29] and a quantum-dot nanostructure.[30,31]

In this paper, we focus on the interaction between vortex light and matter, and study the transfer of vortex light between different light modes. Vortex light carrying OAM has been used to perform information processing. Further quantum and

†Corresponding author. E-mail: banuo2008@163.com
‡Corresponding author. E-mail: wang_lei@jlu.edu.cn

© 2024 Chinese Physical Society and IOP Publishing Ltd

optical networks need to have a network node and quantum repeater, such that the information can be transferred in a controlled way. The interaction of light with matter can provide such a platform, and FWM has been proven to be an effective method for converting the information between different light channels. Thus, we theoretically propose a scheme to obtain the vortex FWM field with OAM in a four-level diamond-configuration atomic system. We found that in the FWM processes, the vortex FWM field can be spatially modulated and the generated FWM mode has a fidelity of approximately 1 by adjusting the corresponding parameters. By tuning the detuning of the probe field, the spatial distribution of the intensity and phase of the vortex FWM field can be effectively controlled. In particular, when the Rabi frequency of the coupled field increases, the intensity of the generated FWM field also increases, and the distorted phase is effectively suppressed. In addition, when the probe field has a certain detuning value, the distorted FWM field can also be suppressed by changing the detuning value of the coupled field.

2. Atomic model and relevant equations

We analyze a four-level diamond-configuration atomic system as shown in Fig. 1. The levels $|1\rangle$, $|2\rangle$, $|3\rangle$ and $|4\rangle$ can correspond to the states $|1\rangle = |5S_{1/2}, F = 2\rangle$, $|2\rangle = |5P_{1/2}, F = 2\rangle$, $|3\rangle = |5P_{3/2}, F = 2\rangle$ and $|4\rangle = |5D_{3/2}, F = 1\rangle$, respectively, in the cold ^{85}Rb. A weak Gaussian pulse field with the Rabi frequency $\Omega_{\rm p} = \Omega_{\rm p0}\exp[-(x^2+y^2)/\omega_{\rm p0}^2]\exp(-t^2/\tau^2)$, where $\omega_{\rm p0}$ and $\Omega_{\rm p0}$ are the transverse waist and initial amplitudes and τ is the pulse width, couples the intermediate level $|2\rangle$ and the ground level $|1\rangle$. A continuous-wave field $\Omega_{\rm c}$ drives the intermediate level $|2\rangle$ and the excited level $|4\rangle$. The intermediate level $|3\rangle$ and the excited level $|4\rangle$ are coupled by an OAM field $\Omega_{\rm v}$, which is defined as

$$\Omega_{\rm v} = \begin{cases} \Omega_{\rm v0}\Omega\,(r)\,{\rm e}^{-{\rm i}\phi l}, \\ \Omega_{\rm v0}\Omega\,(r)\,{\rm e}^{{\rm i}\phi l}, \end{cases} \tag{1}$$

where $\Omega\,(r) = \sqrt{2p!/(\pi\,(p+|l|)!)}\left(\frac{\sqrt{2}r}{\omega_0}\right)^{|l|} L_p^{|l|}\left(\frac{2r^2}{\omega_0^2}\right){\rm e}^{-r^2/\omega_0^2}$, and $\Omega_{\rm v0}$, ω_0, $L_p^{|l|}$, ϕ and $r = \sqrt{x^2+y^2}$ correspond to the amplitude, the beam waist, the Laguerre polynomial, azimuthal angle and the radius, respectively, while l and p represent the azimuthal index and radial index of $L_p^{|l|}$, respectively. In addition, a FWM field $\Omega_{\rm m}$ is generated between level $|1\rangle$ and level $|3\rangle$.

Under the rotating-wave and electric-dipole approximation, with the approximation $\hbar = 1$, the interaction Hamiltonian can be written as

$$\begin{aligned} H_{\rm I} \;=\; & \Delta_{\rm p}|2\rangle\langle 2| + (\Delta_{\rm p}+\Delta_{\rm c}-\Delta_{\rm v})|3\rangle\langle 3| + (\Delta_{\rm p}+\Delta_{\rm c})|4\rangle\langle 4| \\ & - (\Omega_{\rm p}\,{\rm e}^{{\rm i}\boldsymbol{k}_{\rm p}\cdot\boldsymbol{r}}|2\rangle\langle 1| + \Omega_{\rm m}\,{\rm e}^{{\rm i}\boldsymbol{k}_{\rm m}\cdot\boldsymbol{r}}|3\rangle\langle 1| \\ & + \Omega_{\rm c}\,{\rm e}^{{\rm i}\boldsymbol{k}_{\rm c}\cdot\boldsymbol{r}}|4\rangle\langle 2| + \Omega_{\rm v}\,{\rm e}^{{\rm i}\boldsymbol{k}_{\rm v}\cdot\boldsymbol{r}}|4\rangle\langle 3| + {\rm h.c.}). \end{aligned} \tag{2}$$

Here $\Delta_{\rm p} = \omega_{21} - \omega_{\rm p}$, $\Delta_{\rm c} = \omega_{42} - \omega_{\rm c}$, $\Delta_{\rm v} = \omega_{43} - \omega_{\rm v}$ are the detuning of coherent fields and $\Omega_{\rm c} = E_{\rm c}d_{42}/(2\hbar)$ is Rabi frequency of the coupled field. d_{42} represents the transition matrix element from energy level $|4\rangle$ to energy level $|2\rangle$ and k_n ($n = {\rm p}, {\rm m}, {\rm c}, {\rm v}$) are wave vectors and fulfill the phase matching condition $k_{\rm m} = k_{\rm p} + k_{\rm c} + k_{\rm v}$. We use wave vectors to describe the state of atomic system as

$$\begin{aligned} |\Psi\rangle \;=\; & a_1\,|1\rangle + a_2\,{\rm e}^{{\rm i}\boldsymbol{k}_{\rm p}\cdot\boldsymbol{r}}\,|2\rangle + a_3\,{\rm e}^{{\rm i}(\boldsymbol{k}_{\rm p}+\boldsymbol{k}_{\rm c}-\boldsymbol{k}_{\rm v})\cdot\boldsymbol{r}}\,|3\rangle \\ & + a_4\,{\rm e}^{{\rm i}(\boldsymbol{k}_{\rm p}+\boldsymbol{k}_{\rm c})\cdot\boldsymbol{r}}\,|4\rangle\,. \end{aligned} \tag{3}$$

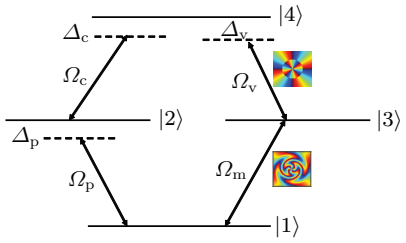


Fig. 1. A four-level atomic scheme with a diamond structure.

Then, with the Schrödinger equation ${\rm d}\,|\Psi\rangle/{\rm d}t = -{\rm i}H_{\rm I}\,|\Psi\rangle$, we can obtain the dynamical equations of atomic probability amplitudes as

$$\begin{aligned} \frac{\partial a_2}{\partial t} &= -{\rm i}\left(\Delta_{\rm p} - {\rm i}\Gamma_2\right)a_2 + {\rm i}\Omega_{\rm c}a_4 + {\rm i}\Omega_{\rm p}a_1, \\ \frac{\partial a_3}{\partial t} &= -{\rm i}\left[\left(\Delta_{\rm p}+\Delta_{\rm c}-\Delta_{\rm v}\right) - {\rm i}\Gamma_3\right]a_3 + {\rm i}\Omega_{\rm v}a_4 + {\rm i}\Omega_{\rm m}a_1, \\ \frac{\partial a_4}{\partial t} &= -{\rm i}\left[\left(\Delta_{\rm p}+\Delta_{\rm c}\right) - {\rm i}\Gamma_4\right]a_4 + {\rm i}\Omega_{\rm c}a_2 + {\rm i}\Omega_{\rm v}a_3, \end{aligned} \tag{4}$$

where Γ_j ($j = 2, 3, 4$) is the decay rate from level $|j\rangle$ to level $|1\rangle$. Considering the slowly varying envelope approximation, the propagation behavior of the probe field and FWM field can be described by the Maxwell equation

$$\begin{aligned} \frac{\partial\Omega_{\rm p}}{\partial z} + \frac{1}{c}\frac{\partial\Omega_{\rm p}}{\partial t} &= {\rm i}\kappa_{\rm p}a_2a_1^*, \\ \frac{\partial\Omega_{\rm m}}{\partial z} + \frac{1}{c}\frac{\partial\Omega_{\rm m}}{\partial t} &= {\rm i}\kappa_{\rm m}a_3a_1^*, \end{aligned} \tag{5}$$

where $\kappa_{\rm p} = 2\pi N\omega_{\rm p}|d_{21}|^2/(\hbar c)$ and $\kappa_{\rm m} = 2\pi N\omega_{\rm m}|d_{31}|^2/(\hbar c)$ are the propagation constants, d_{21} and d_{31} are the electric dipole matrix elements and N is the atomic density. In the limit of a weak probe, the atom is initially prepared in level $|1\rangle$ (i.e., $|a_1|^2 = 1$). Then, Eqs. (4) and (5) are changed into the Fourier form as

$$\begin{aligned} &\left(\omega - \Delta_{\rm p} + {\rm i}\Gamma_2\right)A_2 + \Omega_{\rm c}A_4 + \Omega_{\rm p} = 0, \\ &\left[\omega - \left(\Delta_{\rm p}+\Delta_{\rm c}-\Delta_{\rm v}\right) + {\rm i}\Gamma_3\right]A_3 + \Omega_{\rm v}A_4 + \Omega_{\rm m} = 0, \\ &\left[\omega - \left(\Delta_{\rm p}+\Delta_{\rm c}\right) + {\rm i}\Gamma_4\right]A_4 + \Omega_{\rm c}A_2 + \Omega_{\rm v}A_3 = 0 \end{aligned} \tag{6}$$

and

$$\frac{\partial U_{\rm p}}{\partial z} + \frac{1}{c}\frac{\partial U_{\rm p}}{\partial t} = {\rm i}\kappa_{\rm p}A_2,$$

$$\frac{\partial U_{\rm m}}{\partial z}+\frac{1}{c}\frac{\partial U_{\rm m}}{\partial t}=\mathrm{i}\kappa_{\rm m}A_3, \tag{7}$$

where ω is the Fourier frequency and A_j $(j=2,3,4)$ and $U_{\rm p,m}$ are the Fourier transforms of a_j $(j=2,3,4)$ and $\Omega_{\rm p,m}$, respectively. Using Eq. (6), the solutions are derived as

$$\begin{aligned}A_2&=\frac{M_2\Omega_{\rm p}}{M}+\frac{\Omega_{\rm c}\Omega_{\rm v}\Omega_{\rm m}}{M},\\ A_3&=\frac{\Omega_{\rm v}\Omega_{\rm c}\Omega_{\rm p}}{M}+\frac{M_1\Omega_{\rm m}}{M},\end{aligned} \tag{8}$$

with $M=\gamma_2'\Omega_{\rm v}^2+\gamma_3'\Omega_{\rm c}^2-\gamma_2'\gamma_3'\gamma_4'$, $M_1=\gamma_2'\gamma_4'-\Omega_{\rm c}^2$, $M_2=\gamma_3'\gamma_4'-\Omega_{\rm v}^2$, $\gamma_2'=\omega-\Delta_{\rm p}+\mathrm{i}\Gamma_2$, $\gamma_3'=\omega-\left(\Delta_{\rm p}+\Delta_{\rm c}-\Delta_{\rm v}\right)+\mathrm{i}\Gamma_3$ and $\gamma_4'=\omega-\left(\Delta_{\rm p}+\Delta_{\rm c}\right)+\mathrm{i}\Gamma_4$. By using the initial conditions of the probe field and FWM field, i.e., $U_{\rm p}\left(z=0,\omega\right)\neq 0$ and $U_{\rm m}\left(z=0,\omega\right)=0$, the new FWM field can be obtained as

$$U_{\rm m}\left(z,\omega\right)=U_{\rm p}\left(0,\omega\right)\frac{F_+F_-}{F_--F_+}\left(\mathrm{e}^{\mathrm{i}z\lambda_+}-\mathrm{e}^{\mathrm{i}z\lambda_-}\right), \tag{9}$$

where $F_\pm=\left(k_{\rm p}M_2-k_{\rm m}M_1\pm\sqrt{G}\right)/(2k_{\rm p}M_2\Omega_{\rm c}\Omega_{\rm v})$, $G=\left(k_{\rm p}M_2-k_{\rm m}M_1\right)^2+4k_{\rm m}k_{\rm p}\Omega_{\rm c}^2|\Omega_{\rm v}|^2$ and $\lambda_\pm=\frac{\omega}{c}+\frac{k_{\rm p}M_2+k_{\rm m}M_1}{2M}\pm\frac{\sqrt{G}}{2M}$. The dispersion relations λ_+ and λ_- are used to describe two modes in Eq. (9), in which the λ_- mode is rapidly absorbed after a short propagation distance L, while the λ_+ mode still exists. Then, we give the inverse Fourier transform of $U_{\rm m}$ as

$$U_{\rm m}(L,t)=\begin{cases}\tilde{U}_{\rm m}\,\mathrm{e}^{-\mathrm{i}\phi l}\,\mathrm{e}^{\mathrm{i}L\lambda_+},\\ \tilde{U}_{\rm m}\,\mathrm{e}^{\mathrm{i}\phi l}\,\mathrm{e}^{\mathrm{i}L\lambda_+},\end{cases} \tag{10}$$

where $\tilde{U}_{\rm m}=k_{\rm m}\Omega(r)\Omega_{\rm v0}\Omega_{\rm c}\Omega_{\rm p}(\eta_+)\frac{F_+F_-}{F_--F_+}$, $\eta_+=t-z/\upsilon_{\rm g+}$ and $\upsilon_{\rm g+}=1/\mathrm{Re}\{[\partial\lambda_+]_{\omega=0}\}$ is the group velocity of the λ_+ mode. By using $\lambda_+=\mathrm{Re}(\lambda_+)+\mathrm{i}\,\mathrm{Im}(\lambda_+)$, Eq. (10) can be rewritten as

$$U_{\rm m}(L,t)=\begin{cases}\tilde{U}_{\rm m}\,\mathrm{e}^{-L\mathrm{Im}(\lambda_+)}\,\mathrm{e}^{-\mathrm{i}[\phi l-L\mathrm{Re}(\lambda_+)]},\\ \tilde{U}_{\rm m}\,\mathrm{e}^{-L\mathrm{Im}(\lambda_+)}\,\mathrm{e}^{\mathrm{i}[\phi l-L\mathrm{Re}(\lambda_+)]}.\end{cases} \tag{11}$$

From Eq. (10), we find that $|\tilde{U}_{\rm m}\,\mathrm{e}^{-L\mathrm{Im}(\lambda_+)}|^2$ affects the intensity of the vortex mixing field, while $\mathrm{e}^{\mp\mathrm{i}[\phi l-L\mathrm{Re}(\lambda_+)]}$ determines the distribution pattern and twist direction of the vortex FWM phase in the inner and outer rings, respectively.

3. Numerical calculation and discussion

In this section we discuss the effects of the detuning of two acting fields and the intensity of the coupled field on the phase and intensity of vortex FWM. Figure 2 shows the phase and intensity patterns of the vortex FWM field versus positions x and y for different detunings of the probe field. When the detuning of the probe field is zero, the phase of the vortex FWM field is normal and its strength shows a strong double-ring pattern (see Figs. 2(c) and 2(h)). However, as the absolute value of detuning increases, the phase of vortex FWM field becomes more and more distorted (see Figs. 2(a), 2(b), 2(d) and 2(e)), and its intensity decreases significantly (see Figs. 2(f), 2(g), 2(i) and 2(j)). The above phenomena can be explained by the dispersion relation. In Fig. 3, we point out that when the detuning of the probe field takes different values, the real and imaginary parts of the dispersion λ_+ vary with the radius r. When the detuning of the probe field is resonant (i.e., $\Delta_{\rm p}=0$), the real part of the dispersion is zero, and its imaginary part is lower than 0.10, which makes the phase of the generated vortex FWM normal, and its intensity shows an obvious double-ring structure. When the detuning value of the probe field changes greatly, the imaginary part of the dispersion also increases, indicating that the generated FWM field is absorbed by the medium, so the double-ring structure of intensity becomes weaker. It should be noted that when the detunings of the probe field are negative, the real parts of the dispersion are greater than zero. However, when the detunings of the probe field are positive, the real parts of the dispersion are less than zero. Therefore, it can reasonably explain that the phase distortion direction of FWM in Figs. 2(a) and 2(b) is completely opposite to that in Figs. 2(d) and 2(e).

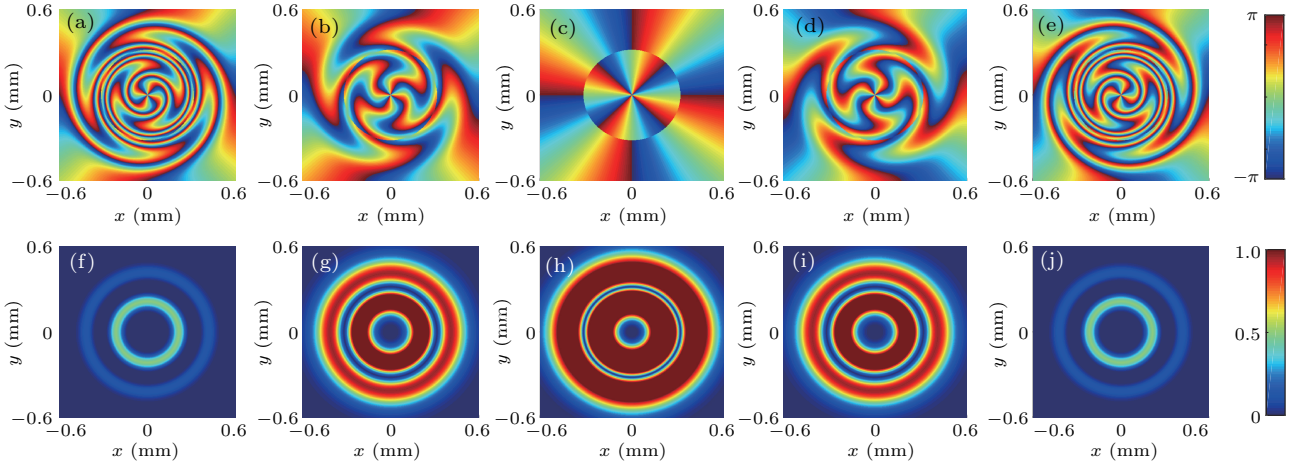


Fig. 2. The phase (a)–(e) and intensity (f)–(j) curves of the vortex FWM field as a function of position when the detuning of the probe field takes different values: (a), (f) $\Delta_{\rm p}=-10\gamma$; (b), (g) $\Delta_{\rm p}=-5\gamma$; (c), (h) $\Delta_{\rm p}=0$; (d), (i) $\Delta_{\rm p}=5\gamma$; and (e), (j) $\Delta_{\rm p}=10\gamma$. The relevant parameters are $\gamma=2\pi$ MHz, $\Gamma_2=0.66\gamma$, $\Gamma_3=5.7\gamma$, $\Gamma_4=6.0\gamma$, $\Omega_{\rm c}=15\gamma$, $\Omega_{\rm v0}=50\gamma$, $L=0.01$ m, $\Delta_{\rm c}=\Delta_{\rm v}=0.0$.

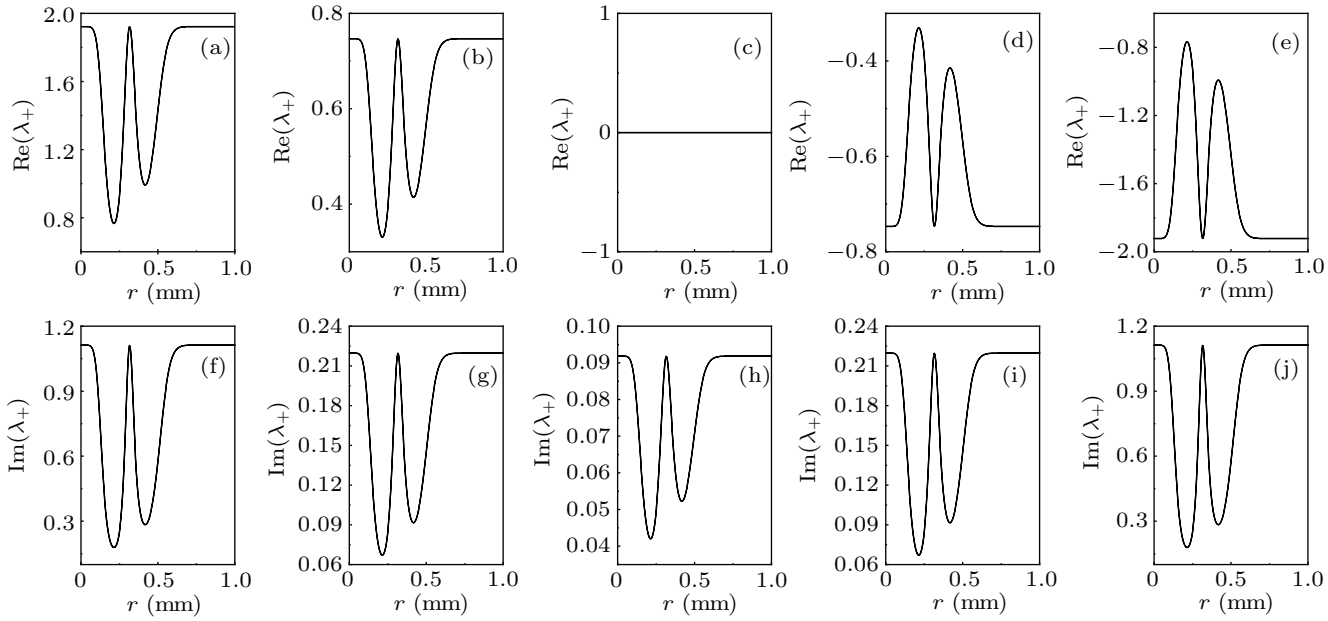


Fig. 3. The real part $\mathrm{Re}\,\lambda_+$ and the imaginary part $\mathrm{Im}\,\lambda_+$ of the dispersion relation versus radius r when the detuning of the probe field takes different values: (a), (f) $\Delta_\mathrm{p} = -10\gamma$; (b), (g) $\Delta_\mathrm{p} = -5\gamma$; (c), (h) $\Delta_\mathrm{p} = 0$; (d), (i) $\Delta_\mathrm{p} = 5\gamma$; and (e), (j) $\Delta_\mathrm{p} = 10\gamma$. The other parameters are the same as those in Fig. 2.

Figure 4 shows the effect of the detuning of the coupled field Δ_c on the vortex FWM when the detuning of the probe field is $\Delta_\mathrm{p} = 10\gamma$. As the detuning value of the coupled field decreases from zero to -4γ, -8γ and -10γ, the phase distortion of the vortex FWM becomes weaker, and its phase returns to normal when the detuning value is -10γ. At the same time, the strength of vortex FWM becomes stronger, and its double-ring structure becomes more and more obvious. In order to explain the above phenomenon, we show the real and imaginary parts of the dispersion, λ_+, versus radius r with different values of Δ_c in Fig. 5. As shown in Fig. 5, when the Δ_c value decreases from zero to -8γ, the amplitude of the real part of the dispersion decreases. When $\Delta_\mathrm{c} = -10\gamma$ meets the two-photon resonance ($\Delta_\mathrm{c} + \Delta_\mathrm{p} = 0$), the real part of the dispersion is very close to zero. Similarly, the imaginary part of the dispersion, i.e., the corresponding absorption, also decreases from zero to -8γ. When the probe field and the coupled field meet the two-photon resonance, the dispersion absorption reaches its minimum value. Therefore, when $\Delta_\mathrm{p} = 10\gamma$, by modulating the detuning of the coupled field the distortion of the FWM phase is suppressed and the strength of the FWM field is greatly improved.

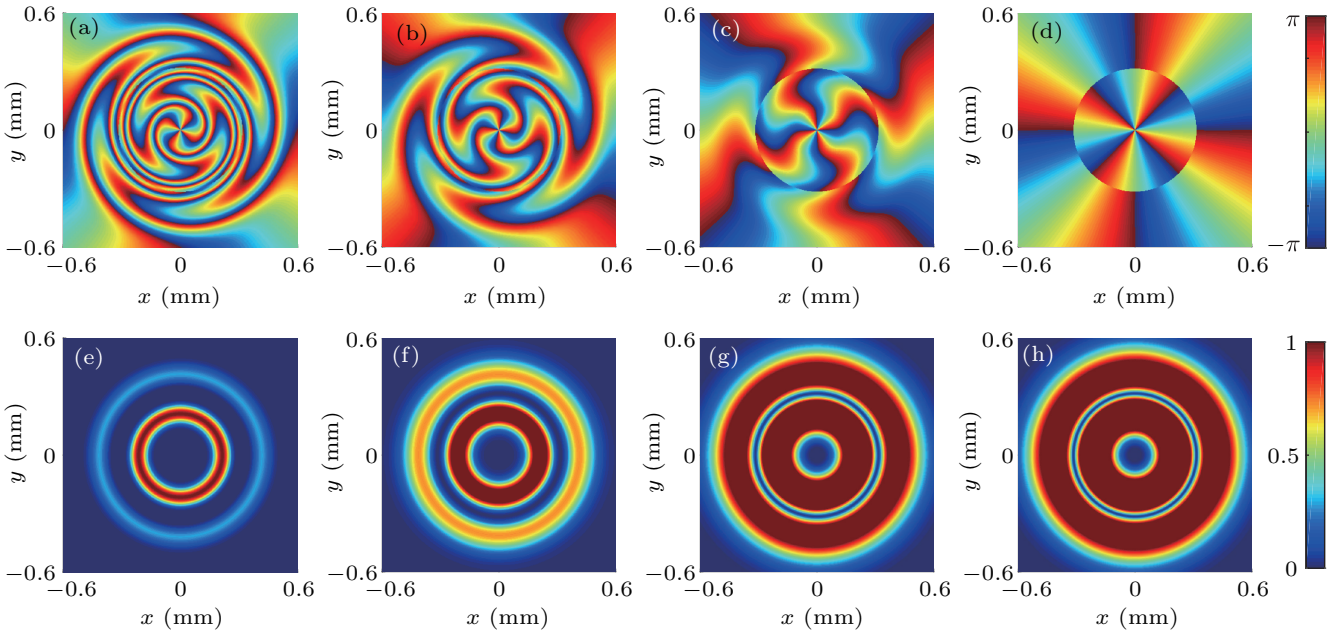


Fig. 4. The phase (a)–(d) and intensity (e)–(h) curves of the vortex FWM field as a function of position for different detunings of the coupled field when $\Delta_\mathrm{p} = 10\gamma$: (a), (e) $\Delta_\mathrm{c} = 0$; (b), (f) $\Delta_\mathrm{c} = -4\gamma$; (c), (g) $\Delta_\mathrm{c} = -8\gamma$; and (d), (h) $\Delta_\mathrm{c} = -10\gamma$. The other parameters are the same as those in Fig. 2.

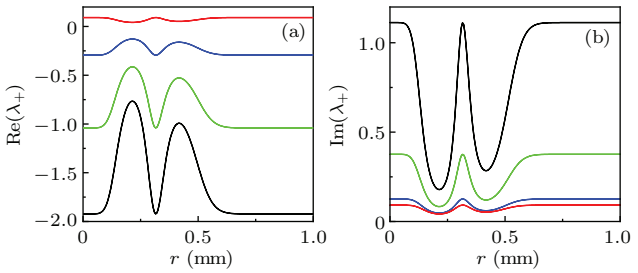


Fig. 5. Real part Reλ_+ and imaginary part Im λ_+ of the dispersion relation vs. radius r when $\Delta_p = 10\gamma$ for different detunings of the coupled field: $\Delta_c = 0$ (black solid), $\Delta_c = -4\gamma$ (green solid), $\Delta_c = -8\gamma$ (blue solid), $\Delta_c = -10\gamma$ (red solid). The other parameters are the same as those in Fig. 2.

Figure 6 shows that when $\Delta_p = 10\gamma$, the phase pattern and intensity distribution of the vortex FWM field are adjusted by increasing the Rabi frequency of the coupling field Ω_c. In Fig. 6, when the detuning of the probe field is 10γ, with the enhancement of the Rabi frequency Ω_c, the degree of phase distortion of the vortex FWM field decreases and finally returns to normal. At the same time, the FWM field becomes stronger and stronger with the increase of Ω_c. Figure 7 shows the real and imaginary parts of the dispersion λ_+ versus radius r for different values of Ω_c. As can be seen, with the enhancement of the Rabi frequency Ω_c, the amplitudes of the real and imaginary parts of the dispersion λ_+ gradually decrease and approach zero.

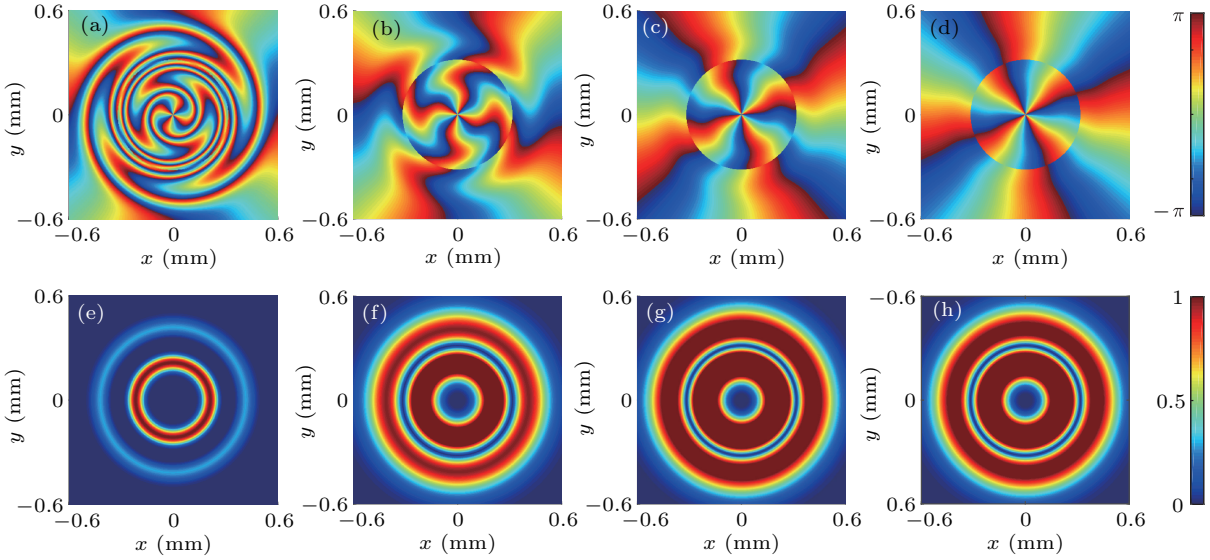


Fig. 6. The phase (a)–(d) and intensity (e)–(h) curves of the vortex FWM field as a function of position for different Rabi frequencies of the coupled field $\Omega_c\gamma$, when $\Delta_p = 10\gamma$: (a), (e) $\Omega_c = 15\gamma$; (b), (f) $\Omega_c = 25\gamma$; (c), (g) $\Omega_c = 35\gamma$; and (d), (h) $\Omega_c = 45\gamma$. The other parameters are the same as those in Fig. 2.

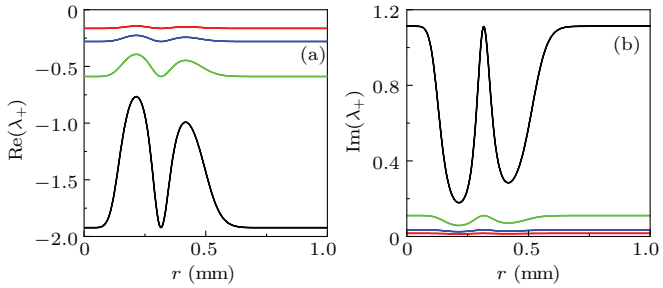


Fig. 7. Real part Re λ_+ and imaginary part Im λ_+ of the dispersion relation versus radius r when $\Delta_p = 10\gamma$ for different Rabi frequencies of the coupled field $\Omega_c\gamma$: $\Omega_c = 15\gamma$ (black), $\Omega_c = 25\gamma$ (green), $\Omega_c = 35\gamma$ (blue), $\Omega_c = 45\gamma$ (red). The other parameters are the same as those in Fig. 2.

We all know that fidelity describes the quality between the generated FWM field and the input angular momentum light. Based on Ref. [32], the fidelity is defined as

$$F = \frac{|\int_x \int_y U_m \Omega_v^* \mathrm{d}x\mathrm{d}y|^2}{\int_x \int_y |U_m|^2 \mathrm{d}x\mathrm{d}y \times \int_x \int_y |\Omega_v|^2 \mathrm{d}x\mathrm{d}y}. \tag{12}$$

Figure 8 shows the change of fidelity F with propagation distance L under different values of detuning of the probe field. When the detection field is resonant with the transition energy level, i.e., $\Delta_p = 0$, the value of fidelity F is close to one, and its value hardly changes with the propagation distance. However, when the detuning value of the probe field increases, the fidelity decreases sharply with propagation distance due to the absorption of the generated FWM field by the system. When the detuning of the probe field has a certain value we can use two methods to improve the fidelity, one is to enhance the strength of the coupling field, Ω_c, and the other is to change the detuning of the coupled field, Δ_c, so that the system meets the two-photon resonance condition. Figure 9(a) shows that when $\Delta_p = 10\gamma$ the fidelity of the FWM field increases as the coupled field strength increases. This result is consistent with Figs. 6 and 7. Due to the enhanced Rabi frequency of the coupled field, the coherence between the field and the atom is enhanced, and the EIT phenomenon becomes apparent, resulting in large FWM fidelity values. In addition, Fig. 9(b) shows how to increase the fidelity of FWM by changing the detuning value of the coupling field when $\Delta_p = 10\gamma$. As shown in Fig. 9(b), when the probe field and coupled field satisfy two-photon resonance (i.e., $\Delta_p + \Delta_c = 0$), the fidelity of FWM reaches the maximum value and is approximately equal to one.

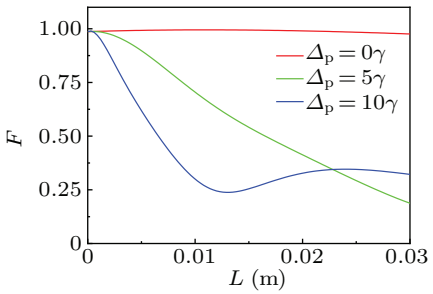


Fig. 8. Normalized fidelity F of the vortex FWM field versus propagation distance L for different detunings of the probe field: $\Delta_p = 0$ (black), $\Delta_p = 5\gamma$ (green), $\Delta_p = 10\gamma$ (red). The other parameters are the same as those in Fig. 2.

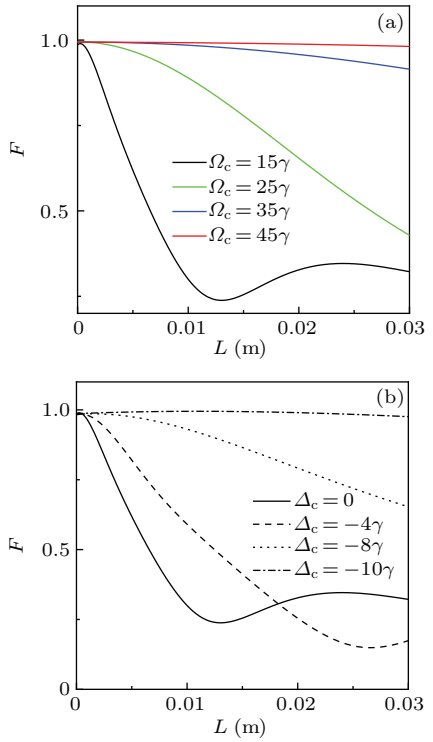


Fig. 9. (a) Normalized fidelity F of the vortex FWM field versus propagation distance L for different Rabi frequencies of the coupled field Ω_c: $\Omega_c = 15\gamma$ (black), $\Omega_c = 25\gamma$ (green), $\Omega_c = 35\gamma$ (blue), $\Omega_c = 45\gamma$ (red). (b) Normalized fidelity of the vortex FWM field versus propagation distance for different detunings of the coupled field: $\Delta_c = 0$ (solid curve), $\Delta_c = -4\gamma$ (dashed curve), $\Delta_c = -8\gamma$ (dotted curve), $\Delta_c = -10\gamma$ (dash-dotted curve). The other parameters are the same as those in Fig. 2.

4. Conclusion

In conclusion, we have investigated a four-level diamond-configuration atomic system for realizing a spatially correlated vortex four-wave mixing field. It is found that under the slow light mechanism, the phase and intensity modes of orbital angular momentum can be transferred from the coupled field to the generated four-wave mixing field. By changing the detuning value of the probe field, the spatial pattern of the intensity and phase of the vortex four-wave mixing field can be controlled. It is worth noting that when the probe field has a large detuning value, in order to achieve a high intensity and an untwisted vortex mixing field, on the one hand, it is possible to enhance the Rabi frequency of the coupled field; on the other hand, the detuning value of the coupled field can be changed to satisfy the two-photon resonance condition. Finally, we further study the influence of the above parameters on the fidelity of the four-wave mixing field and find that when the probe field has a certain detuning value, the fidelity can only be increased and approach 1 by increasing the Rabi frequency of the coupled field or making the system satisfy two-photon resonance. Our research may be applied to the field of quantum optics and quantum information based on orbital angular momentum.

Acknowledgements

Project supported by the National Natural Science Foundation of China (Grant Nos. 11704151 and 11247201) and the Twelfth Five-year Program for Science and Technology of Education Department of Jilin Province (Grant No. 20150215).

References

[1] Gray H R, Whitley R M and Stroud C R 1978 *Opt. Lett.* **3** 218
[2] Scully M O, Zhu S Y and Gavrielides A 1989 *Phys. Rev. Lett.* **62** 2813
[3] Gao J Y, Zhang H Z, Cui H F, Guo X Z, Jiang Y, Wang Q W, Jin G X and Li J S 1994 *Opt. Commun.* **110** 590
[4] Harris S E 1997 *Phys. Today* **50** 36
[5] Fleischhauer M, Imamoglu A and Marangos J P 2005 *Rev. Mod. Phys.* **77** 633
[6] Harris S E, Field J E and Imamoglu A 1990 *Phys. Rev. Lett.* **64** 1107
[7] Hakuta K, Marmet L and Stoicheff B P 1991 *Phys. Rev. Lett.* **66** 596
[8] Zhang G Z, Hakuta K and Stoicheff B P 1993 *Phys. Rev. Lett.* **71** 3099
[9] Jain M, Yin G Y, Field J E and Harris S E 1993 *Opt. Lett.* **18** 998
[10] Li Y Q and Xiao M 1996 *Opt. Lett.* **21** 1064
[11] Deng L, Kozuma M, Hagley E W and Payne M G 2002 *Phys. Rev. Lett* **88** 143902
[12] Wu Y, Saldana J and Zhu Y 2003 *Phys. Rev. A* **67** 013811
[13] Wu Y, Payne M G, Hagley E W and Deng L 2004 *Opt. Lett.* **29** 2294
[14] Zhang Y, Brown A W and Xiao M 2007 *Phys. Rev. Lett.* **99** 123603
[15] Allen L, Beijersbergen M W, Spreeuw R J C and Woerdman J P 1992 *Phys. Rev. A* **45** 8185
[16] He H, Friese M E J, Heckenberg N R and Rubinsztein-Dunlop H 1995 *Phys. Rev. Lett.* **75** 826
[17] Hamedi H R, Ruseckas J, Paspalakis E and Juzeliūnas G 2019 *Phys. Rev. A* **99** 033812
[18] Wang H H, Wang J, Kang Z H, Wang L and Gao J Y 2019 *Phys. Rev. A* **100** 013822
[19] Hamedi H R, Paspalakis E, Žlabys G, Juzeliūnas G and Ruseckas J 2019 *Phys. Rev. A* **100** 023811
[20] Walker G, Arnold A S and Franke-Arnold S 2012 *Phys. Rev. Lett.* **108** 243601
[21] Zhang W, Ding D S and Jiang Y K 2014 *Appl. Phys. Lett.* **104** 171103
[22] Wang Z G, Yang J W, Sun Y Y and Zhang Y P 2018 *Opt. Lett.* **43** 4354
[23] Pan X Z, Yu S, Zhou Y F, Zhang K, Zhang K, Lv S C, Li S J, Wang W and Jing J T 2019 *Phys. Rev. Lett.* **123** 070506
[24] Qiu J, Wang Z P, Ding D S, Huang Z X and Yu B L 2020 *Phys. Rev. A* **102** 033516
[25] Yin H, Wang Z P, Ding D S and Yu B L 2019 *Opt. Express* **27** 29863
[26] Yu C and Wang Z P 2021 *Phys. Rev. A* **103** 013518
[27] Wang Z P, Zhang Y F, Paspalakis E and Yu B L 2020 *Phys. Rev. A* **102** 063509
[28] Qiu J, Wang Z P, Ding D S, Li W B and Yu B L 2020 *Opt. Express* **28** 2975
[29] Zhang Y F, Wang Z P, Qiu J and Yu B L 2019 *Appl. Phys. Lett.* **115** 171905
[30] Rahmatullah, Abbas M, Ziauddin and Qamar S 2020 *Phys. Rev. A* **101** 023821
[31] Mahdavi M, Sabegh Z A, Mohammadi M, Mahmoudi M and Hamedi H R 2020 *Phys. Rev. A* **101** 063811
[32] Liu R, Li F, Padgett M J and Phillips D B 2015 *Optica* **2** 1028